Proceedings of the Thirty-third (2023) International Ocean and Polar Engineering Conference **www.isope.org**
Ottawa, Canada, June 19-23, 2023

ISBN 978-1-880653-80-7; ISSN 1098-6189

CFD Study of Interaction among Wave, Current and a Fixed Cylinder

*Bo Han, Weiwen Zhao, Decheng Wan**

Computational Marine Hydrodynamic Lab (CMHL), School of Naval Architecture, Ocean and Civil Engineering,
Shanghai Jiao Tong University, Shanghai, China
*Corresponding author

ABSTRACT

Accurate prediction of hydrodynamic performance under complex sea conditions is of great significance to engineering safety. A numerical study on the interaction among waves, current and a fixed cylinder is presented in this paper, and the simulation is conducted with the *naoe-FOAM-SJTU* solver, a viscosity solver for hydrodynamics based on OpenFOAM independently. The flow field is seriously influenced by the generation of a regular wave and current and the strong non-linear interaction caused by viscosity among them and a single fixed cylinder.
In this paper, a mesh convergence study is conducted at prior, and a proper set of mesh is chosen according to that. Furthermore, the simultaneous generation of the regular wave and current is realized with the boundary of numerical field, and the propagation of the wave is also validated. The results of wave elevation and pressures captured by the wave gauges and probes around the fixed cylinder are compared with the experiment results. Along with the comparison of different working conditions, some unique phenomena and features of the wave-current-cylinder working condition can be identified and analyzed.

KEY WORDS: wave-current interaction; numerical simulation; naoe-FOAM-SJTU solver

INTRODUCTION

The research of sea condition is always a crucial issue for the coastal and offshore structure design. The economic losses resulting from the coastal and offshore structure accident are too large to be afforded, so surviving from the predicted harshest sea condition is one of the final aims of structure design. Therefore, accurate prediction of complex working conditions is of great significance to the safety and economics of offshore structure design. Two types of wave-current interactions are identified and the influence are analyzed (Wang et al, 2022).
On the other hand, in energetic areas, waves and tidal currents interact for modifying the energy resource and impacting on the design conditions (Ayumi et al, 2013). The sea condition we can describe more complex, the profits we can estimate more exactly.
In the sea, waves and currents typically occur together, creating complex flow patterns that can subject offshore structures to increased loads and forces. While research on the analysis of extreme waves (Saincher et al, 2022) and structures (Han et al, 2021), the vortex mechanism of interaction between currents and structure (Chen et al, 2022), and the modeling of wave-current interactions has made significant progress (Blondeaux et al, 2015), structures that experience the interaction of waves and currents are becoming increasingly common and require further investigation (Ghadirian et al, 2021). It is crucial to understand the physics of wave-current interactions and accurately predict the loads and forces that offshore structures will experience under these conditions. Furthermore, the impact of wave-current interactions on the marine ecosystem is also an important consideration. Therefore, designing offshore structures that minimize their impact on the marine environment is a critical aspect of responsible engineering. Overall, further research is needed to improve our understanding of wave-current interactions and their effects on offshore structures and the marine ecosystem.

The CFD solver *naoe-FOAM-SJTU* is developed based on OpenFOAM to solve the problems in marine engineering with viscosity and incompressible fluid assumption (Shen et al, 2016). In the present work, numerical simulations of the interaction among waves, current and fixed cylinder and corresponding validations are realized on the *naoe-FOAM-SJTU* solver. The results and the phenomena are compared with the other working conditions. The comparisons show the unique performances of the interaction of wave, current and cylinder.

NUMERICAL METHODS

Governing Equations

The numerical simulation is conducted on the CFD solver *naoe-FOAM-SJTU* based on the assumption of the incompressible fluid. In the present work, the large eddy simulation (LES) is chosen as the turbulence model, and the governing equations should be written as follows:

$$\nabla\cdot\mathbf{U}=0 \tag{1}$$

$$\frac{\partial\rho\mathbf{U}}{\partial t}+\nabla\cdot(\rho\mathbf{U}\mathbf{U})=-\nabla p_d-\mathbf{g}\cdot\mathbf{x}\nabla\rho+\nabla\cdot\left\{\rho\nu_{sgs}\left[\nabla\mathbf{U}+(\nabla\mathbf{U})^T-\frac{1}{3}(\nabla\cdot\mathbf{U})\mathbf{I}\right]\right\}-\frac{2}{3}\rho k\mathbf{I} \tag{2}$$

where **U** is velocity; ρ is density of the fluid which is mixed by the two phases of air and water; p_d is the dynamic pressure; **x** is position vector; k is turbulent kinetic energy; **I** is identity matrix; ν_{sgs} is the kinematic viscosity of the sub-grid scale eddies, it can be calculated as

$$\nu_{sgs} = (C_S \Delta)^2 \sqrt{2 S_{ij} S_{ij}} \tag{3}$$

in which, C_S is known as the Smagorinsky coefficient; Δ is the scale of the grid; S_{ij} is the component of the strain rate tensor.

Interface Capturing Method

In two-phase simulations in the present work, the free surface is captured by the volume of fluid (VOF) method. The method is mainly dependent on the volume fraction α, which indicates the volume ratio of each grid. The volume fraction at the current time step can be updated by

$$\frac{\partial \alpha}{\partial t} + \nabla \cdot \mathbf{U}\alpha + \alpha(1-\alpha)\nabla \cdot \mathbf{U}_c = 0 \tag{4}$$

In which $\mathbf{U}_c = \min\left[c_\alpha |\mathbf{U}|, \max(|\mathbf{U}|)\right] \frac{\nabla \alpha}{|\nabla \alpha|}$, where constant c_α is a compression factor and takes value 1 by default.

Wave Generation

The wave condition in the present work is regular wave, and the Stokes second wave theory is chosen for the wave generation. The theoretical free surface height of the Stokes second wave is

$$\eta = \frac{H}{2}\cos(\theta) + k\frac{H^2}{4}\frac{3-\tanh^2(kh)}{4\tanh^3(kh)}\cos(2\theta) \tag{5}$$

where H is designed wave height; θ is phase of the wave; k is wave number; h is the depth of the wave tank.

In the present work, both wave and current contribute to the main working condition, therefore the influence of current is also demand to be taken into consideration. The horizontal and vertical free surface velocity components under wave and current are

$$u = \frac{H}{2}\omega\frac{\cosh(kz)}{\sinh(kh)}\cos(\theta) + \frac{3}{4}\frac{H^2\omega k\cosh(2kz)}{4\sinh^4(kh)}\cos(2\theta) + u_{current} \tag{6}$$

$$w = \frac{H}{2}\omega\frac{\sinh(kz)}{\sinh(kh)}\sin(\theta) + \frac{3}{4}\frac{H^2\omega k\sinh(2kz)}{4\sinh^4(kh)}\sin(2\theta) \tag{7}$$

in which, ω is angular velocity of the wave; $u_{current}$ is velocity of the current.

NUMERICAL SETUP

Computational Domain

The main parameters of the computational domain and the wave-current working condition is listed in Table 1, and Fig. 1 gives a more intuitive perspective of the computational domain and the cylinder. The size of the whole domain is set as -7.45 m ~ 7.45 m, -1.1 m ~ 1.1 m and -0.7 m ~ 0.7 m in *x*, *y* and *z* direction.

As to the boundary condition, the wave generation and inflow is set at the inlet boundary, and the corresponding wave absorption is also set at the outlet boundary. The no-slip boundary condition is adopted to the bottom and the cylinder boundary, the Neumann boundary condition is applied to the atmosphere boundary, and the symmetry boundary condition is imposed on the both sides of the computational domain.

Table 1. Parameters of the computational domain and wave-current interaction working condition

Parameter	Value
Depth	0.7 m
Wave height	0.2 m
Wave length	7.45 m
Wave period	3 s
Current velocity	0.34 m/s
Cylinder diameter	0.22 m

Probes Preset

In order to measure the variable height of the free surface, wave gauges are necessary to set up before the numerical simulation. Fig. 2 shows the horizontal distribution of the wave gauges, and the specific locations of them are listed in Table 2. A wave gauge (WP1) is set relatively near to the inlet boundary to monitor the correction of the wave propagation. Three wave gauges is set (WP2 ~ 4) to observe the variation of the wave shape, and there are 5 wave gauges (WP5 ~ 9) located around the cylinder on the other side used for capture the wave run-up around the cylinder.

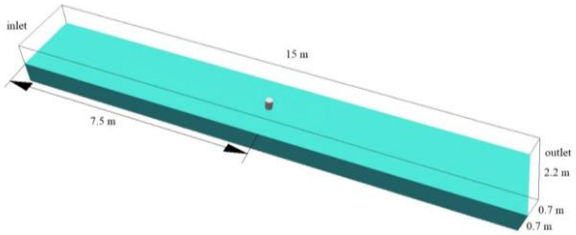

Fig. 1. Computational domain

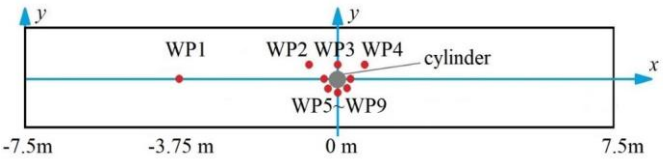

Fig. 2. The horizontal location sketch of wave gauges

Table 2. Specific horizon locations of wave gauges

Wave gauge number	*x* (m)	*y* (m)
WP1	-3.72500	0.00000
WP2	-0.57000	0.61500
WP3	0.00000	0.61500
WP4	0.57000	0.61500
WP5	-0.11500	0.00000
WP6	-0.08132	0.08132
WP7	0.00000	0.11500
WP8	0.08132	0.08132
WP9	0.11500	0.00000

Wave run-up around induces drastic changes of the pressure around the cylinder near the free surface, therefore pressure data is helpful to explain the movement of free surface and understand the interaction of wave and current. Some positions around the cylinder are interested in and chosen to preset the pressure probes as Fig. 3, and the specific

coordinates of them are listed in the Table 3. Four pressure probes (PP1 ~ 4) are set on the wave-ward side at different heights the same as the experiment, five pressure probes (PP2 and PP5 ~ 8) are set at the same height and 45° intervals around the cylinder in the horizontal direction,

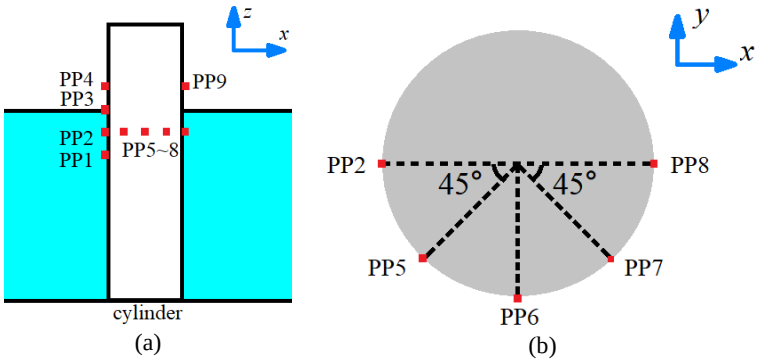

Fig. 3. The locations sketch of pressure probes from (a) side view and (b) vertical view

and a pressure probe (PP9) is set at the same height of PP4 on the wave-back side of the cylinder to monitor the convergence phenomenon of the wave passing the both sides of the cylinder.

Table 3. Specific locations of pressure probes

Pressure probe number	x (m)	y (m)	z (m)
PP1	-0.115	0	-0.185
PP2	-0.115	0	-0.085
PP3	-0.115	0	0.015
PP4	-0.115	0	0.115
PP5	-0.08132	0.08132	-0.085
PP6	0	0.115	-0.085
PP7	0.08132	0.08132	-0.085
PP8	0.115	0	-0.085
PP9	0.115	0	0.115

Computational Mesh

In order to guarantee the high-fidelity numerical simulation conducted, proper computational mesh is important. In the present work, the commercial software Pointwise is adopted to generate the structured mesh for numerical simulation, which is shown in Fig. 4. On the whole, in terms of cells distribution, the closer its position to the cylinder, the denser the mesh designed to capture the flow field as fine as possible with finite computing resources. In Fig. 4 (b), an O-grid block is chosen to fit the shape of cylinder with structed-mesh, and the radius of the block is designed as 0.42 m. Besides, according to some experimental simulations, the cells near free surface (-0.1 m$\leqslant$ z $\leqslant$ 0.25 m) are refined specially, which is smaller than 1/40 of the wave height. There are totally 6,975,094 cells in the mesh.

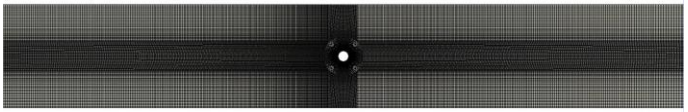

(a)

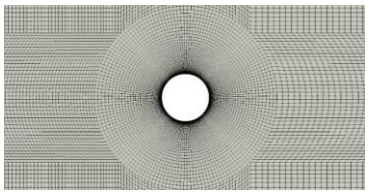

(b)

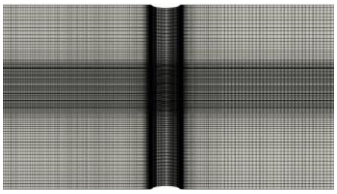

(c)

Fig. 4. Computational mesh (a) overview on x-y plane at z = 0, (b) magnified view on x-y plane at z = 0, and (c) magnified view on x-z plane at y = 0

Numerical Schemes

In the present work, the finite-volume method is used to conduct the numerical simulation following the OpenFOAM platform. The temporal term, is discretized with the first-order Euler scheme. In terms of the spatial discretization, the SIMPLE algorithm is adopted to decouple the velocity and the pressure. Then preconditioned conjugate gradient (PCG) solver solves the pressure equation with the diagonal incomplete-Cholesky (DIC) preconditioner. As to other variables, such as velocity and phase fraction α, they are handled by a solver implemented by symmetric Gauss-Seidel smoother. The tolerances of all of the solvers are set lower than 10^{-5} to reduce the dimensions of residuals.

Considering the wave and the inflow velocity, the time step is set small enough as 0.00025 s to ensure the maximum Courant number lower than 1. According to the experimental simulation, the wave-current-cylinder interaction phenomenon reaches a stable state from about the time that the third peak passing the cylinder. Thus, the duration of the whole simulation is set as 24 s, which is equal to 8 periods, to keep at least 5 stable periods.

MESH CONVERGENCE STUDY AND WAVE VALIDATION

Mesh Convergence Study

The numerical simulation is conducted on 3 sets of 2-dimentional meshes with same working condition of wave and current (shown as Table 1) but the existence of cylinder in the same CFD time of 24 seconds, in order to check out which one fits the simulation best. Table 4 lists the grid sizes and clock time of the 3 sets of meshes, and Fig. 5 compares the wave elevation historical curves in two complete stable periods at WP1 of 3 sets of meshes.

Table 4 Parameters of 3 sets 2-dimensional mesh in mesh convergence study

Mesh number	N_t	Δx (m)	Δz (m)	Clock time (s)
1	2.7×10^4	0.0157	0.021	34380
2	6.9×10^4	0.0078	0.011	117576
3	9.9×10^4	0.0039	0.005	121824

In Table 4, N_t is the total cells number of the mesh; Δx is the uniform horizontal cell size of the O-grid region around the position of cylinder; Δz is the uniform vertical cell size of the refinement region around the free surface.

According to the Fig. 5, it can be observed that the wave elevation amplitude of mesh 1 is slightly smaller than the other two sets of meshes due to the numerical dissipation. Referring the suggested procedure of Celik et al., the amplitude data of the wave elevation historical curves of the 3 sets of meshes are taken into the grid convergence index (GCI) study, as shown in Table 5. In light of Table 4, grid refinement factor r is 2. Through the calculation, the converge ratio is known smaller than 1, which confirms the solution is monotonic convergence with the refinement of the mesh. Furthermore, the numerical uncertainty defined by grid convergence index (GCI) also shrinks with the gradual refinement of the meshes, and GCI_{23} is lower than 5%. Thus, we adopt the grid design and distribution of mesh 2 to generate 3-dimensional mesh in the following numerical simulation and analysis.

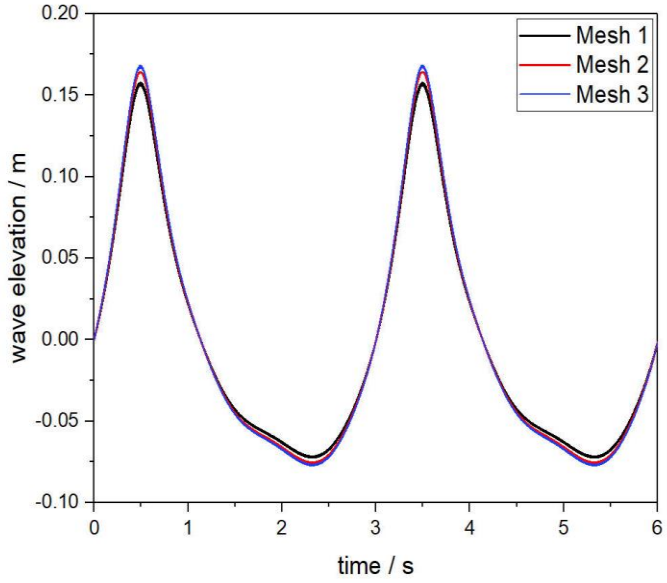

Fig. 5. Wave elevation historical curves in two complete stable periods at WP1 of 3 sets of meshes

Table 5 Grid convergence index (GCI) study for the wave elevation amplitudes

Parameter	Value
ε_{12}	-0.00713 m
ε_{23}	-0.00457 m
r	2
Converge ratio	0.641
p	0.642
GCI_{12}	6.629%
GCI_{23}	4.249%

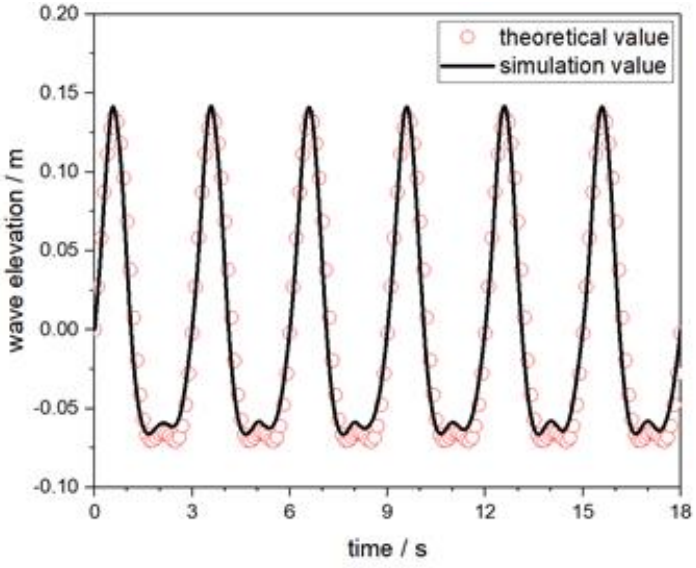

Fig. 6. Wave elevation historical curves of regular wave test and theoretical solution at the position of WP1

Wave Validation

We confirmed the grid convergency of the solution and chose the proper grid strategy in the last section. Now it is clear that the numerical simulation has a result with low numerical uncertainty, but the solution is correct or not still remains to be validate. A regular wave test without structure is performed with 3-dimensional mesh adopting the grid strategy and numerical setup above. The parameters of the regular wave are identical to the wave condition, and the theoretical solution can be calculated based on it. The result of the test is compared with the theoretical solution according to equation (5) in Fig. 6. The relative error of the simulation value is lower than 3% in stable periods, which indicates the availability of numerical setup and grid adaptation in terms of the present working condition.

RESULT AND DISCUSSION

Fig. 7 shows the free surface around the cylinder under the working condition of the interaction of wave and current. The ripples in Fig. 7 (a)(b) looks like the type-1 ripple in the phenomenon “ringing” as a circle taking the cylinder as the center, and ripples in Fig .8 (c)(d) looks like the type-2 ripple as two circles on the sides of cylinder. However, if the ripples are regarded as “ringing”, some difference can still be pointed out. Fig.9 shows the same period of the interaction between cylinder and wave only as Fig. 7. It can be easily observed that, when it is compared with the real “ringing” in Fig. 8, the “type-2” ripples in Fig. 7 (c) occur later than that in Fig. 8 (b), and the shape of “type-1” ripples in Fig. 7 (b) is much more obvious than the Fig. 8 (a). The wave steepness of present working condition is lower than 0.03, and according to Mosheni et al.,when it is increased to 0.0625, the type-1 ripple of “ringing” in the working condition of interaction between cylinder and wave only can be clearly observed. The differences above are considered caused by different generation reason of ripples. The “ringing” is just a phenomenon occurs when the peak of wave passing the structure, while the ripples in the working condition under the interaction of wave and current mainly affected by the wave resistance brought by the current, which takes much more mechanical energy.

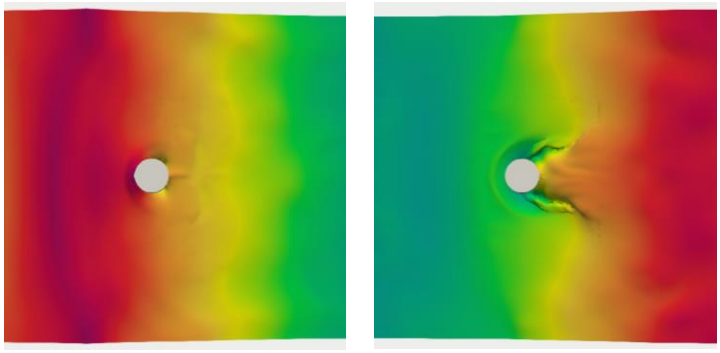

(a) $t = n\mathrm{T} + \mathrm{T} / 4$ (b) $t = n\mathrm{T} + \mathrm{T} / 2$

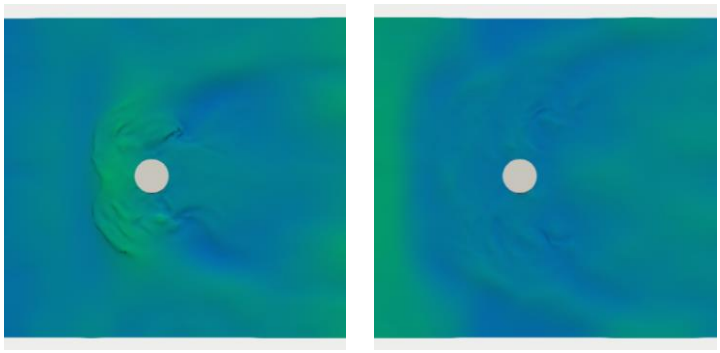

(c) $t = n\mathrm{T} + 3\mathrm{T} / 4$ (d) $t = n\mathrm{T}$

Fig. 7. Vertical view of free surface around the cylinder under the working condition of the interaction of wave and current

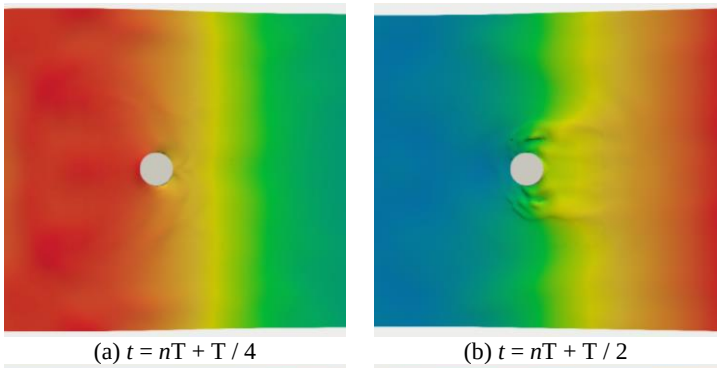

(a) $t = n\mathrm{T} + \mathrm{T} / 4$ (b) $t = n\mathrm{T} + \mathrm{T} / 2$

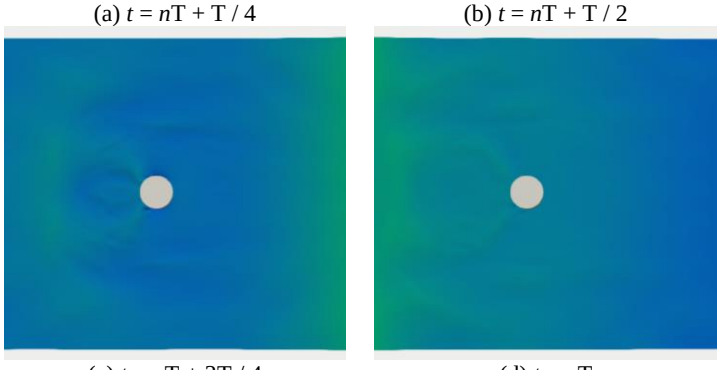

(c) $t = n\mathrm{T} + 3\mathrm{T} / 4$ (d) $t = n\mathrm{T}$

Fig. 8. Vertical view of free surface around the cylinder under the working condition of wave

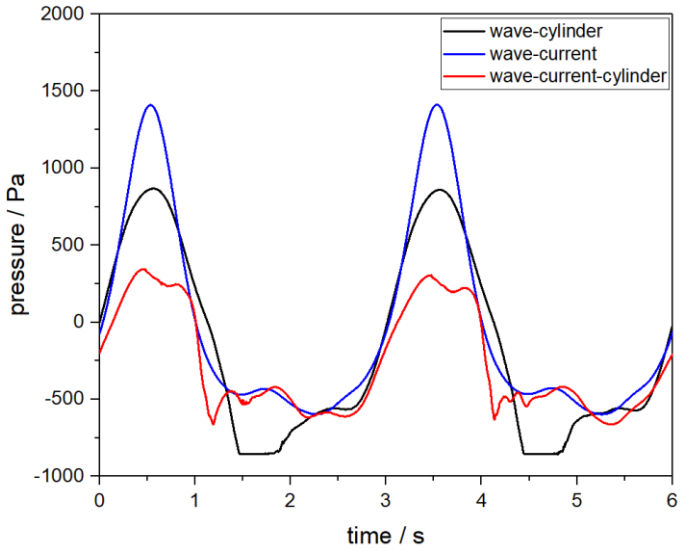

Fig. 9. Pressure historical curves of the side of cylinder (PP6)

Fig. 9 shows the dynamic pressure comparison of the side of cylinder under different working conditions combinations of wave, current and cylinder of the same parameters. According to the table 3, PP6 is installed at z = -0.085 m, which is above the free surface when meets the trough of the wave-cylinder working condition, therefore, the dynamic pressure historical curve displays as a line segment. From the comparison, the amplitude of pressure under wave-current-cylinder working condition is obviously lower than the other, and the shape of the curve is much more complex than the other: the hollow on peak of the curve and the fluctuation of the trough. This is also a performance of the loss of mechanical energy, and these can be understood through the specific phenomena as follows:

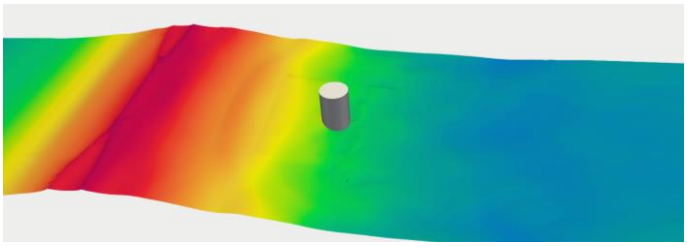

Fig. 10. Wave approaches the cylinder under the wave-current-cylinder working condition

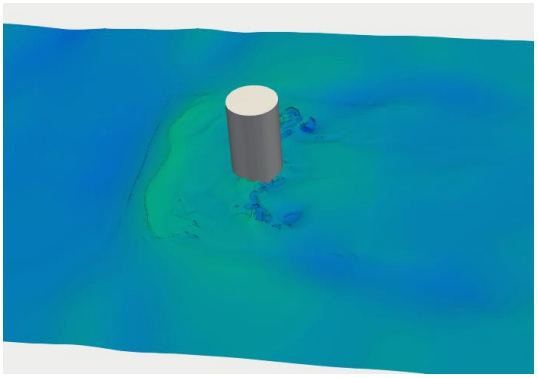

Fig. 11 Wave breaking after the wave passing the cylinder under the wave-current-cylinder working condition

Fig. 10 shows the scene that wave approaches the cylinder in the wave-current-cylinder working condition. The peak of the wave has already obviously deformed before passing the cylinder. Fig. 11 shows the phenomenon looks like wave breaking on the side of cylinder after the wave peak passing it. These unique phenomena explain the special shape of peak and trough in pressure historical curve of the wave-current-cylinder condition respectively.

CONCLUSIONS

In the present work, the numerical simulation of the interaction among wave, current and fixed cylinder is conducted with *naoe-FOAM-SJTU* solver. We take proper mesh through the mesh convergence study and validate the wave propagation with the theoretical solution. As to the result of simulation, we compare the pressure and the phenomena of the working condition of wave-current-cylinder with wave-current and wave-cylinder working conditions. The pressure historical curve of the wave-current-cylinder working condition has lower amplitude and different fluctuations, and the unique phenomena can also be observed such as the wave has already deformed before the peak passing the cylinder, wave breaking occurs on the sides of cylinder after the peak passing cylinder, which can provide proper explanation for the different pressure curve. These phenomena take place in the wave-current-cylinder working condition only, and along with obvious complex flow mechanism such as wave breaking, which points out the importance of taking viscosity into consideration.

ACKNOWLEDGEMENTS

This work was supported by the National Natural Science Foundation of China (52131102), and the National Key Research and Development Program of China (2019YFB1704200), to which the authors are most grateful.

REFERENCES

Blondeaux P. , Vittori G. , et al. (2015). A simple model of wave-current interaction[J]. Journal of Fluid Mechanics, 775: 328-348.

Chen, S. , Zhao, W. , & Wan, D. . (2022). Turbulent structures and characteristics of flows past a vertical surface-piercing finite circular cylinder. Physics of fluids(1 Pt.3), 34.

Ghadirian, A. , Vested, M. H. , Carstensen, S. , Christiensen, E. D. , & Bredmose, H. . (2021). Wave-current interaction effects on waves and their loads on a vertical cylinder. Coastal Engineering, 165, 103832.

Han, B. , Zhao, W. , & Wan, D. . (2021). Numerical study on interaction between focusing waves with fixed cylinder. International Journal of Offshore and Polar Engineering, 31(1), 95-101.

Higuera, P. , Lara, J. L. , & Losada, I. J. . (2013). "Realistic wave generation and active wave absorption for navier–stokes models: application to openfoam". Coastal Engineering, 71.

Hildebrandt, A. , Sriram, V. , & Schlurmann, T. . (2013). "Simulation of focusing waves and local line forces due to wave impacts on a tripod structure". International Offshore & Polar Engineering Conference.

Lin, P. , & Li, C. W. . (2003). Wave-current interaction with a vertical square cylinder. Ocean Engineering, 30(7), 855-876.

Longuet-Higgins, M.S.. (1974). "Breaking waves - in deep or shallow water," 10th Symp. Naval Hydrodynamics. 597-605.

Mohammad, M. , Esperanca, P. T. , & Sphaier, S. H. . (2018). Numerical study of wave run-up on a fixed and vertical surface-piercing cylinder subjected to regular, non-breaking waves using openfoam. Applied Ocean Research, 79, 228-252.

Rusche, H., (2002). "Computational Fluid Dynamics of Dispersed Two-Phase Flows at High Phase Fractions", Ph.D.Thesis, Imperial College, London, UK.

Saincher S. , Sriram V. , Agarwal S. et al. (2022). Experimental investigation of hydrodynamic loading induced by regular, steep non-breaking and breaking focused waves on a moving cylinder. 2022, 93: 42-64

Saruwatari, A. , Ingram, D. M. , & Cradden, L. . (2013). Wave-current interaction effects on marine energy converters. Ocean Engineering, 73(6), 106-118.

Shen, Z., Wan, D. (2016). "An irregular wave generating approach based on naoe-FOAM-SJTU solver." China Ocean Eng 30, 177–192

Tambroni, N. , Blondeaux, P. , & Vittori, G. . (2015). A simple model of wave-current interaction. Journal of Fluid Mechanics, 775, 328-348.